The solution structure of HIV-1 Nef reveals an unexpected fold and permits delineation of the binding surface for the SH3 domain of Hck tyrosine protein kinase

Stephan Grzesiek[1], Ad Bax[1], G. Marius Clore[1], Angela M. Gronenborn[1], Jin-Shan Hu[1], Joshua Kaufman[2], Ira Palmer[2], Stephen J. Stahl[2] and Paul T. Wingfield[2]

The solution structure of HIV-1 Nef has been solved by multidimensional heteronuclear NMR spectroscopy. The construct employed to circumvent problems associated with aggregation was a double-deletion mutant (Δ2–39, Δ159–173) in which conformationally disordered regions of the protein at the N terminus and in a long solvent-exposed flexible loop were removed, without affecting the properties or structural integrity of the remainder of the protein. Despite the absence of any sequence similarity, the overall fold of Nef is reminiscent of that of the family of winged helix-turn-helix DNA binding proteins. The binding surface of Nef for the SH3 domain of Hck tyrosine protein kinase has been mapped and reveals a non-contiguous (in terms of amino-acid sequence) interaction surface. This unique feature may suggest possible avenues for drug design aimed at inhibiting the interaction between Nef and SH3 domains.

[1]Laboratory of Chemical Physics, Building 5, National Institute of Diabetes and Digestive and Kidney Diseases, National Institutes of Health, Bethesda, Maryland 20892, USA
[2]Protein Expression Laboratory, Building 6B, National Institute of Arthritis and Musculoskeletal Diseases, National Institutes of Health, Bethesda, Maryland 20892, USA

Nef is a 27, 000 M_r regulatory factor that is unique to the primate lentiviruses and plays a key role in human immunodeficiency virus (HIV) infection and pathogenicity[1,2]. Indeed, a recent study of the HIV-1 sequences of a cohort of long-term (greater than 10 years) survivors with no signs of clinical progression to acquired immunodeficiency syndrome (AIDS) and with normal CD4 counts, revealed the consistent presence of deletions within the nef gene[3,4], confirming previous studies on macaques that simian immunodeficiency virus (SIV) with the nef gene deleted replicates poorly, does not cause disease, and provides protection against infection by pathogenic SIV[2,5]. Thus, Nef represents a possible target for structure-based rational anti-HIV drug design. To this end we have solved the three-dimensional solution structure of HIV-1 Nef and mapped the interaction surface for the binding of SH3 domains by multidimensional NMR spectroscopy.

Nef is expressed at particularly high levels early after HIV-1 infection, when its mRNA accounts for more than three-quarters of the total viral mRNA[6]. While the precise role of Nef at the molecular level has not been fully established, structure–function studies indicate that Nef has at least two separable activities: down-regulation of the CD4 receptor and enhancement of viral replication[7]. Endocytosis of CD4 involves the interaction of Nef with a dileucine motif in the cytoplasmic tail of CD4, which competes with the binding of lymphocyte-specific protein tyrosine kinase p56lck[8] to CD4, thereby possibly interfering with signalling through the interleukin-2 receptor[9]. This activity of Nef is dependent on the presence of an N-terminal membrane targeting sequence (residues 2–7) and a conserved glutamic acid-rich region (residues 60–71)[7]. Enhancement of infectivity, on the other hand, is dependent on the presence of an intact Pro-X-X-Pro repeat from residues 69–78, reminiscent of an SH3 target site[7]. The absence of this polyproline repeat, however, has no effect on down-regulation of CD4[7]. In this regard, it has recently been shown that intact Nef binds specifically and with submicromolar affinity to the SH3 domain of a subset of Src family kinases, in particular Hck and to a lesser extent Lyn[10,11]. This interaction may be related to the promotion of viral replication by Nef[10,12].

Structure determination

The structure of Nef was solved by three- and four-dimensional double and triple resonance NMR spectroscopy making use of uniformly ^{15}N, $^{15}N/^{13}C$ and $^{15}N/^{2}H$-labelled protein[13,14]. In addition to the commonly used array of experiments, we found that a 4D $^{15}N/^{15}N$-separated nuclear Overhauser enhancement spectrum recorded on a $^{15}N/^{2}H$-labelled sample in H_2O was particularly useful[15], both for sequential assignment and delineation of secondary structure elements. Since all protein variants employed were only sufficiently soluble at pH values greater than 8, it was essential to use methodology that preserved bulk solvent magnetization[16], in order to obviate the effect of rapid exchange of the backbone amide protons with solvent. Full length Nef tends to aggregate[17] and we did not find conditions under which it was monomeric above ~0.1 mM. Preliminary data indicated that the first 50 residues did not adopt an ordered conformation. Deletion of residues 2–39 ($Nef^{\Delta 2-39}$) yielded a protein with considerably better properties (monomeric up to about 0.6 mM), albeit at pH values (≥8, without affecting the chemical shifts of the remaining resonances and therefore without perturb-

ing the structure. However, the apparent rotational correlation time τ_c, derived from ^{15}N relaxation measurements, was too long to permit a full three-dimensional structure determination. The initial studies on $Nef^{\Delta 2-39}$ revealed the presence of a long, flexible and partially solvent-exposed loop comprising residues 148–180. Further deletion of residues 159–173 resulted in the $Nef^{\Delta 2-39,\Delta 159-173}$ construct which displayed identical resonance positions to $Nef^{\Delta 2-39}$ for the remaining residues (that is, the structure is unaltered), had the same affinity for the SH3 domain of Hck as the full length Nef, and exhibited a τ_c of ~12 ns at 35 °C. Although the decrease in τ_c was modest, since it is manifested in all dimensions of the NMR spectra, it was sufficient to permit nearly complete ^1H, ^{13}C and ^{15}N assignments to be obtained. Nevertheless, the observed value of τ_c remains nearly 50% larger than one might expect for a globular approximately spherical protein of this molecular weight (~18,000 M_r). Analytical ultracentrifugation indicates that this is not due to dimerization but rather to non-specific aggregation.

The three-dimensional structure of $Nef^{\Delta 2-39,159-173}$ was obtained by simulated annealing[18] on the basis of 1183 experimental NMR restraints comprising NOE-derived interproton distance, torsion angle, $^3J_{HN\alpha}$ coupling constant and secondary carbon chemical shift restraints. Although the number of NOE derived interproton distance restraints employed was relatively small (640), it is important to note that these included only 24 intraresidue NOE restraints. The total number of NOE restraints could have been increased by a factor of 1.5–2 by including many more easily assignable intraresidue interproton distance restraints. However, the structural information contained within the approximate intraresidue interproton distance restraints is only useful at high resolution when the average number of NOE restraints per residue exceeds ~15. In this particular case, inclusion of additional intraresidue NOE restraints would have been of little consequence to the precision, accuracy or quality of the structures. A superposition of the final 40 simulated annealing structures is shown in Fig. 1 and a summary of the structural statistics is provided in Table 1. The precision of the coordinates is 0.90±0.07 Å for the backbone atoms, 1.44±0.25 Å for all atoms and 1.10±0.20 Å for all atoms of internal side chains (excluding the poorly defined regions of the protein which comprise the N-terminal methionine and residues 40–67 at the N terminus, residues 200–206 at the C terminus, and residues 148–180 which form the long loop connecting strands β4 and β5). All φ,ψ backbone torsion angles within the ordered parts of the protein lie within the allowed region of the Ramachandran plot.

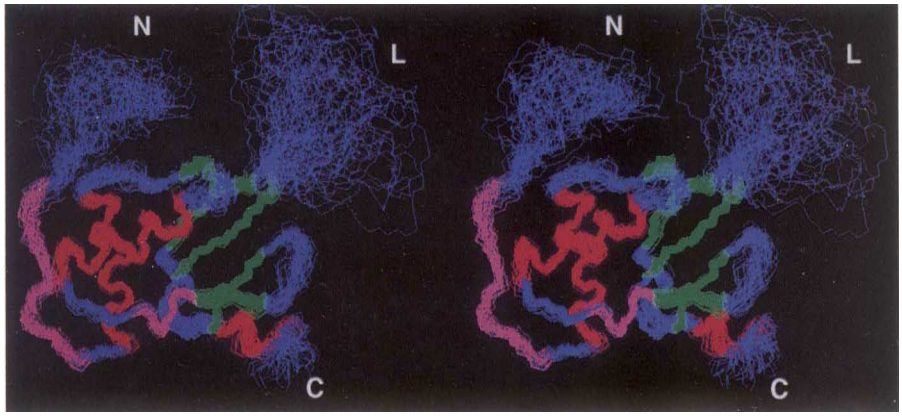

Fig. 1 Superposition of the backbone (N, Cα, C) atoms (residues 56–201) of the final 40 simulated annealing structures of $Nef^{\Delta 2-39,\Delta 159-173}$. The helices are displayed in red, the β-strands in green, the polyproline helix and the short helical turn in magenta, and the rest in blue.

Description of the structure of Nef

Backbone ribbon drawings and the packing of internal side chains of $Nef^{\Delta 2-39,\Delta 159-173}$ are shown in Figs 2*a-c*. The structure comprises a polyproline helix (residues 69–78), three helices (residues 81–94, 105–118 and 194–198), and a five-stranded antiparallel β-sheet (residues 100–102, 126–128, 134–137, 142–146 and 181–186) arranged in a +4x, -1, -1, -1 topology. Strand β1 is located between helices 1 and 2. Strands β2 and β3, β3 and β4, and β4 and β5 are connected by a five-residue loop, a four-residue turn and a conformationally disordered 19-residue loop (34 residues in $Nef^{\Delta 2-39}$), respectively. The polyproline helix lies on top of helix 2 and is stabilized by a number of hydrophobic interactions comprising Val 66, Phe 68, Val 70 and Thr 71 at the start of the polyproline helix and Ile 109, Leu 112, Trp 113 and Thr 117 of helix 2. α-helices 1 and 2 are oriented at an angle of ~105° and helix–helix contacts are formed by Ala 83, Ala 84, Leu 87, Leu 91, Leu 110 and Ile 114. Helices 1 and 2 lie on top of the β-sheet and the hydrophobic core of the protein is formed by Met 79, Ala 83, Leu 87, Leu 91, Leu 97, Leu 110, Ile 114, Tyr 120, Trp 124, Tyr 127, Pro 136, Thr 138, Trp 141, Tyr 143, Leu 145, Leu 181 and Trp 183. The third helix is packed against the back side of strands β2 and β3 in the view shown in Fig. 2*b* with hydrophobic interactions involving Pro 129, Ile 133, Tyr 135, Pro 136, Leu 137, Leu 189, Ala 195, Leu 198 and Pro 200. The N terminus (residues 40–68) preceding the polyproline helix forms a long disordered loop which appears to fold back on the loop connecting helix 1 and strand β1 as shown by several unambiguous NOEs between Trp 57 and Leu 97.

We also examined two other Nef deletion variants (data not shown): the $Nef^{\Delta 2-52}$ deletion displayed identical resonance positions and similar linewidths as $Nef^{\Delta 2-39}$, whereas the $Nef^{\Delta 2-59}$ deletion mutant exhibited very broad lines (with a τ_c of ~20 ns). Thus, in the absence of Trp 57, a hydrophobic patch is formed on the surface of the protein which presumably promotes self-association. Interestingly, HIV-1 protease cleaves Nef at the Trp 57–Leu 58 peptide bond[19].

Comparison of Nef sequences from various sources suggests which residues are likely to be

Table 1 Structural statistics[1]

Structural statistics	<SA>
R.m.s deviations from experimental distance restraints (Å)[2]	
All (702)	0.096±0.006
interresidue sequential (li – jl = 1) (305)	0.079±0.009
interresidue short range (1 < li – jl ≤5) (95)	0.099±0.016
interresidue long range (li – jl) > 5) (216)	0.095±0.011
intraresidue (24)	0.124±0.031
H-bonds (62)	0.144±0.016
R.m.s. deviations from $^3J_{HN\alpha}$ coupling constants (Hz) (91)[2]	0.73±0.06
R.m.s. deviations from exptl dihedral restraints (°) (161)[2,3]	0.61±0.17
R.m.s. deviations from exptl secondary shifts (p.p.m.)	
$^{13}C\alpha$ (119)	1.28±0.06
$^{13}C\beta$ (110)	1.27±0.10
Deviations from idealized covalent geometry	
bonds (Å) (2270)	0.005±0.0003
angles (°) (4101)	0.56±0.03
impropers (°) (1260)[4]	0.46±0.03
E_{L-J} (kcal•mol^{-1})[5]	-517±16
Coordinate precision (Å)[6]	
backbone atoms	0.90±0.07
all atoms	1.44±0.25
all atoms of internal residues	1.10±0.20

[1]The notation of the NMR structures is as follows: <SA> is the ensemble of the final 40 simulated annealing (SA) structures; $\overline{SA}$ is the mean structure obtained by averaging the coordinates of the individual SA structures best fitted to each other using residues 58–147 and 181–199. The number of terms for the various restraints is given in parentheses.
[2]None of the structures exhibit distance violations greater than 0.7 Å, dihedral angle violations greater than 5°, or $^3J_{HN\alpha}$ coupling constant violations greater than 2 Hz;. For each backbone hydrogen bond there are two distance restraints: $r_{NH\text{-}O}$, 1.7–2.5 Å; $r_{N\text{-}O}$, 2.3–3.5 Å.
[3]The dihedral angle restraints comprise 128ϕ, 10ψ, 9χ1 and 14 aromatic χ2 angles.
[4]The improper torsion restraints serve to maintain planarity and chirality.
[5]E_{L-J} is the Lennard-Jones van der Waals energy calculated with the CHARMM empirical energy function[34] and is not included in the target function for simulated annealing or restrained minimization.
[6]The coordinate precision is defined as the average atomic r.m.s. difference between the individual simulated annealing structures and the mean coordinates $\overline{SA}$. Values are reported for residues 68–147 and 181–199. The N-terminal methionine and residues 40–67 at the N terminus, residues 200–206 at the C terminus, and residues 148–180, which form the long solvent exposed loop connecting strands β4 and β5, are disordered.

structurally and functionally important. Sequences of Nef from different HIV-1 isolates as well as different primate lentiviruses reveal the presence of five conserved regions comprising residues 64–90 (block A), 91–96 (polypurine tract), 106–114 (block B), 130–148 (block C) and 179–190 (block D)[1,20]. Each of these conserved blocks comprises elements of secondary structure. Thus, the polyproline helix and helix 1 are located in block A and the polypurine tract, helix 2 in block B, strands β3 and β4 in block C, and strand β5 in block D.

Comparison with proteins with related folds

The overall fold of Nef$^{\Delta 2-39,\Delta 159-173}$ is reminiscent of that of the family of winged helix-turn-helix (HTH) DNA-binding proteins, which includes the catabolite gene activator protein of *Escherichia coli*, HNF3/forkhead, the ETS family of transcription factors, the heat shock transcription factor and the globular domain of histone H5 (GH5). There is, however, an important difference: the DNA recognition helix of the HTH motif is absent in Nef$^{\Delta 2-39,\Delta 159-173}$, where it is replaced by an extended segment of polypeptide chain (residues 119–121) and a four-residue helical turn (residues 122–125) that connect helix 2 to strand β2. The closest structural similarity is with GH5[21] (Fig. 2*d*), where it is possible to superimpose 40 Cα atoms of Nef$^{\Delta 2-39,\Delta 159-173}$ and GH5 within an atomic r.m.s. difference of ~2 Å (specifically, residues 83–90, 107–120, 121–126, 142–147 and 181–186 of Nef$^{\Delta 2-39,159-173}$ onto residues 27–34, 47–60, 64–69, 80–85 and 91–96 of GH5). This structural alignment comprises helices 1 and 2, the short helical turn leading into strand β2, and strands β4 and β5 of Nef$^{\Delta 2-39,\Delta 159-173}$, and helices 1 and 2, the first four residues of helix 3 (the recognition helix of the HTH motif), and strands β2 and β3 of GH5. GH5 has a three-stranded antiparallel β-sheet with a +2x, –1 topology and the three strands correspond to strands β1, β4 and β5 of Nef$^{\Delta 2-39,\Delta 159-173}$ (that is, strands β2 and β3 of Nef are missing in GH5). Despite the above described structural similarity, the percentage sequence identity is only 7.5%. Nevertheless, the pattern of hydrophobic and hydrophilic residues, perhaps not surprisingly, tends to be conserved. The significance of this structural similarity cannot as yet be ascertained. It is possible that Nef evolved from a DNA-binding transcription factor of the winged HTH variety which subsequently lost the recognition helix of the HTH motif as a result of a deletion leading to a shortening of the polypeptide chain between helix 2 and strand β2.

Mapping the interaction surface for Hck SH3

The recent reports of the formation of a specific high-affinity complex (K_D≈0.3 μM) between the SH3 domain of Hck and Nef[11] led us to study this interaction by NMR. While the biological consequences of the interaction with Nef and the SH3 domain of Hck have not been elucidated, two observations lead one to believe that this interaction is biologically significant. First, the polyproline binding site (residues 69–78) for the SH3 domain of Hck[11] has been shown to be critically related to the enhancement of infectivity[7]. Second, the affinity of Nef for the SH3 domain of Hck is approximately two orders of magnitude higher than that for other SH3–target interactions[11], strongly suggesting that this interaction is not an accident of nature.

At substoichiometric concentration of Hck-SH3, two sets of resonances for Nef are observed, one corresponding to unligated Nef$^{\Delta 2-39}$, the other to the Nef$^{\Delta 2-39}$–Hck-SH3 complex. This indicates that the complex is long-lived on the NMR time scale (with a lifetime greater than 50 ms, and a K_D<<1 μM, assuming a diffusion-limited on-rate of 10^8 M^{-1}s^{-1}). Further, since the affinity of Nef$^{\Delta 2-39}$ for Hck SH3 is similar to that of full length Nef[11], any involvement in binding of the unstructured N-terminal domain (residues 2–39) is unlikely. The same slow chemical exchange behaviour (K_D<<1 μM) is observed for the complex of Nef$^{\Delta 2-39,\Delta 159-173}$ and Hck-SH3. In addition, the pattern of chemical shift changes induced on binding of

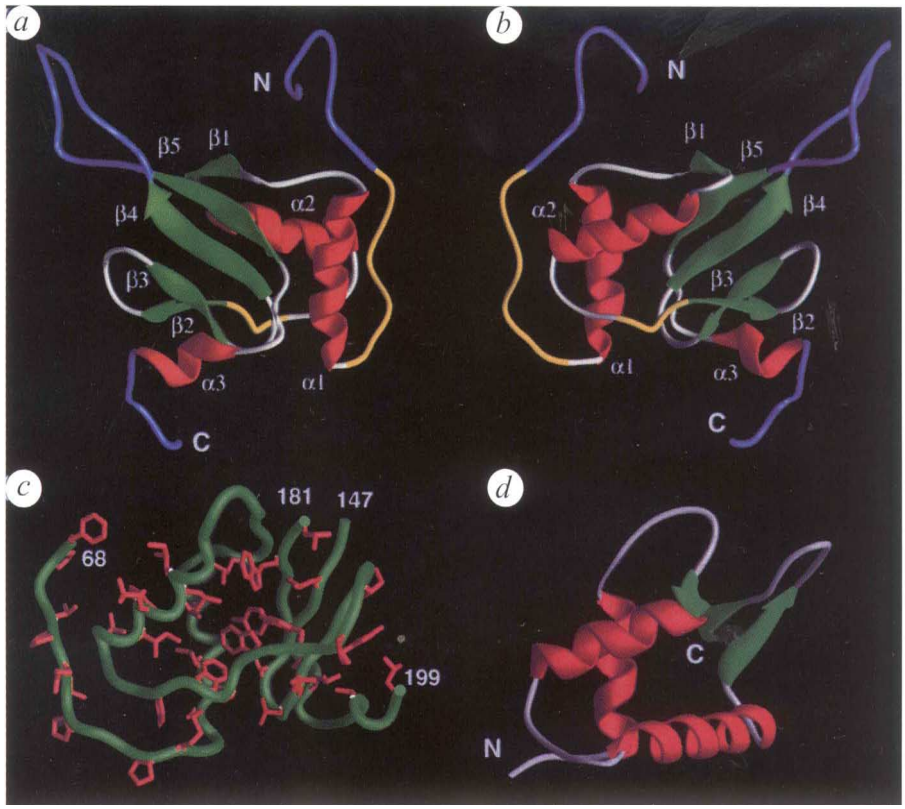

Fig. 2 *a* and *b*, Two views showing a backbone ribbon diagram of $Nef^{\Delta 2-39,\Delta 159-173}$ (residues 56–206). *c*, Packing of the hydrophobic core of $Nef^{\Delta 2-39,159-173}$. *d*, Backbone ribbon diagram of GH5[21] in the same orientation as (*b*) showing the similar fold to $Nef^{\Delta 2-39,159-173}$. The colour coding in (*a*), (*b*) and (*d*) is as follows: helices, red; β-strands, green; polyproline helix and helical turn preceding strand β2, yellow; ordered loops, grey; and disordered regions, blue. In (*c*) the backbone for residues 68–147 and 181–199 is shown as a green worm and the internal side chains are shown in red. (*a*), (*b*) and (*d*) were generated with the program RIBBONS[32] and (*c*) with the program GRASP[33].

the SH3 domain is identical for the two constructs (unpublished data). In summary, this indicates that full length Nef, $Nef^{\Delta 2-39}$ and $Nef^{\Delta 2-39,\Delta 159-173}$ bind the SH3 domain of Hck in the same manner.

The residues whose NH, ^{15}N, $^{13}C\alpha$ and $^{13}C\beta$ resonances are most affected upon binding are colour coded in Fig. 3*a* on a tubular representation of the backbone of $Nef^{\Delta 2-39,\Delta 159-173}$. The largest backbone chemical shift changes are observed for Gln 73 and Val 74, followed by His 116, Arg 77, Phe 121, Asp 86 and Val 70. This delineates a concave interaction surface on $Nef^{\Delta 2-39,\Delta 159-173}$ bounded by the polyproline helix and helix 1. The floor

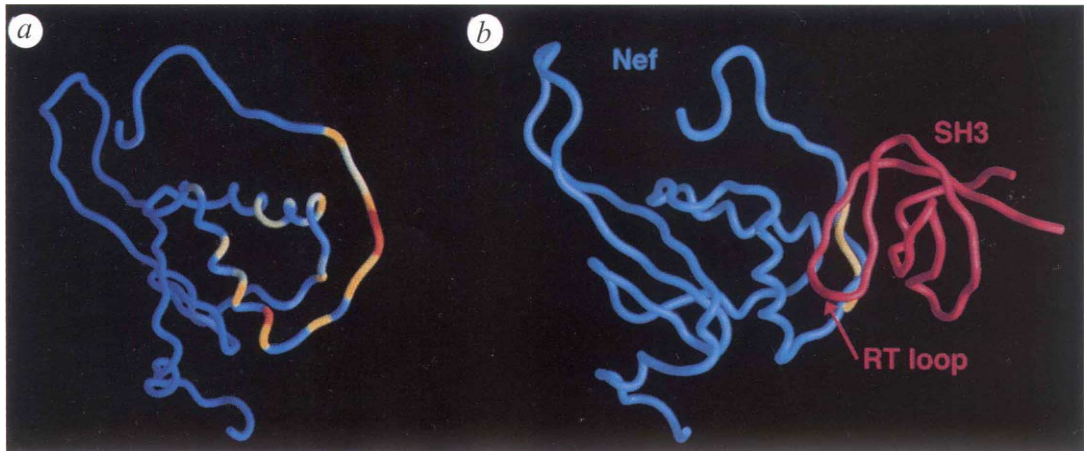

Fig. 3 Model for the interaction of $Nef^{\Delta 2-39,\Delta 159-173}$ with the SH3 domain of Hck. *a*, A backbone worm of $Nef^{\Delta 2-39,\Delta 159-173}$ (residues 56–206) is displayed colour coded to show those residues whose backbone NH, ^{15}N, $^{13}C\alpha$ and $^{13}C\beta$ resonances are most affected on binding the SH3 domain of Hck. The mean shift difference Δ_{ave} for each amino acid was calculated as $0.25[(\Delta_{NH})^2 + (\Delta_N/5)^2 + (\Delta_{C\alpha}/2)^2 + (\Delta_{C\beta}/2)^2]^{1/2}$ where Δ_i is the chemical shift difference for resonance i in the free and complexed states. The colours range from red (Δ_{ave}=1.0), through yellow (Δ_{ave}=0.4), to blue (Δ_{ave}(0.1). Two residues of Nef, Pro 77 and Ala 83, could not be assigned in the complex and are colour-coded in orange. *b*, A model of the complex obtained by docking the SEM-5-peptide complex[22] onto $Nef^{\Delta 2-39,\Delta 159-173}$ by best fitting residues 1–7 of the peptide with residues 71–77 of $Nef^{\Delta 2-39,\Delta 159-173}$ (see text). The colour coding is as follows: $Nef^{\Delta 2-39,\Delta 159-173}$, blue; the SH3 domain of SEM-5, red; and the nine-residue peptide (PPPVPPRRR) from mSos, yellow. This figure was generated with the program GRASP[33].

of this concave surface is formed by the C-terminal end of helix 2 and the short segment of extended polypeptide following helix 2. These data also imply a critical role for the Pro_{72}–Gln–Val–Pro_{75} stretch of the polyproline segment (residues 69–78), in complete agreement with both mutagenesis data—which indicate that substitution of either Pro 72 or Pro 75 of Nef by Ala abolishes its binding to Hck-SH3—and comparative binding data on Nef from SIV which still binds Hck-SH3 with high affinity despite the fact that the two outer prolines at positions 69 and 78 are substituted by Ser and Thr respectively[10]. The presence of Val 74 and Arg 77 (which are conserved in all Nef sequences from HIV and SIV[1]) at the P_0 and P_{-3} binding positions indicates that the polyproline helix of Nef binds to Hck-SH3 in the minus orientation[21–23]. With this information in hand, we modelled the complex of $Nef^{\Delta 2-39,\Delta 159-173}$ with Hck-SH3 by the best fitting of residues Thr_{71}–Pro–Gln–Val–Pro–Leu–Arg_{77} of $Nef^{\Delta 2-39,\Delta 159-173}$ onto residues 1–7 (PPPVPPR) and residues 2–8 (PPALPPK) of the polyproline peptides (comprising the P_3 to P_{-3} binding positions) complexed with the SH3 domains of SEM5[22] and c-Crk[24], respectively. In both cases a fit of ~1.5 Å was obtained and the resulting orientation of the SH3 domain relative to Nef is the same. The model for a Nef–SH3 complex obtained in this manner is displayed in Fig. 3*b*. It can be seen that the RT loop (the RT loop connects strands 1 and 2 of the SH3 domain and is named in this manner because it contains critical Arg and Thr residues in the tyrosine kinase Src) of the SH3 domain is directed towards helix 1, as well as the floor of the binding pocket. This would account for the observation that short polyproline peptides derived from $Nef^{\Delta 2-39,\Delta 159-173}$ only bind weakly to Hck-SH3[10], indicating that other contacts between Nef and Hck-SH3 are required for high affinity binding. The model is also consistent with the finding that Ile 69 of the RT loop of the SH3 domain of murine Hck is a critical determinant of high affinity binding and that its substitution by a polar residue (Asp or Arg) reduces the affinity by at least two orders of magnitude[10]. In our model, the side chain of Ile 69 of the RT loop is directed towards Ile 114 of Nef located in the floor of the binding pocket. Introduction of a charged side chain at position 69 of the RT loop of the SH3 domain would therefore bury a charge, resulting in an energetically unfavourable situation.

In conclusion, we have solved the solution structure of HIV-1 Nef, and shown that it has a topology very similar to that of the winged helix-turn-helix transcription factors. The availability of this structure will permit the rational pursuit of structure-function studies on Nef. While the present structure of Nef has not been determined to very high precision it still provides an important guide and source of ideas for drug design. Specifically, the competitive inhibition of SH3 binding seems a promising target. The mapping of the interaction surface presented in this paper is crucial for such an endeavour as it reveals a novel mode of SH3 binding that has not been previously observed, namely that the binding surface on Nef is not comprised of contiguous amino acids. This unique feature relative to other known SH3–target interactions immediately suggests avenues for drug design.

Methods

Sample preparation. Various derivatives of HIV-1 Nef (strain BH10) containing a Cys 206→Ala mutation and an N-terminal methionine as residue 1 were produced in *E. coli* using the T7 expression system[25]. The DNA encoding the protein was generated as an NdeI–BamHI fragment using the polymerase chain reaction as described in ref. 26 and cloned into the expression vector pET11a[25]. The variants expressed were as follows: full length Nef, deletions of residues 2–39 ($Nef^{\Delta 2-39}$), 2–52 ($Nef^{\Delta 2-52}$) and 2–59 ($Nef^{\Delta 2-59}$), and a deletion of residues 2–39 and a part of a long solvent exposed loop comprising residues 159–173 ($Nef^{\Delta 2-39,\Delta 159-173}$). (The sequence numbering used for Nef is the same as that given in ref. 1.). The SH3 domain of murine Hck tyrosine-protein kinase (residues 60–116 plus an N-terminal methionine) was generated from a cDNA clone[27] and cloned into pET11a[25]. Protein expression from the pET constructs in *E. coli* strain DE3 was induced with 2 mM IPTG for 3.5 h. Labelling with ^{15}N, ^{13}C and/or ^{2}H was carried out by growing the bacteria on minimal medium using $^{15}NH_4Cl$, $^{13}C_6$-glucose and $^{2}H_2O$ as the sole nitrogen, carbon and deuterium sources, respectively. Cells were lysed using a French press and proteins purified from the soluble extract by anion exchange chromotography followed by gel filtration.

NMR spectroscopy and structure determination. Samples for NMR contained approximately 0.6 mM protein, pH 8. All NMR spectra were recorded on a Bruker AMX600 spectrometer equipped with an 8 mm self-shielded *z* gradient triple resonance probe (Nalorac). Approximate interproton distance restraints were derived from 3D heteronuclear separated NOE spectra (mixing time 70 ms) on protonated samples and from a 4D $^{15}N/^{15}N$-separated NOE spectrum (mixing time 200 ms) on a perdeuterated sample, and torsion angle restraints from analysis of the NOE and coupling constant data[13]. Coupling constants were obtained by means of quantitative *J*-correlation spectroscopy[28]. Structures were calculated by hybrid distance geometry-simulated annealing[18] using the program X-PLOR[29] modified to incorporate restraints for $^{3}J_{HN\alpha}$ coupling constants[30] and $^{13}C\alpha$ and $^{13}C\beta$ chemical shifts[31]. The target function minimized comprises harmonic potentials for covalent geometry (bonds, angles and improper torsions), coupling constants and carbon chemical shifts; quadratic square-well potentials for interproton distance and dihedral angle restraints; and a quartic van der Waals repulsion term for the non-bonded contacts.

The coordinates have been deposited in the Brookhaven Protein Data Bank. The accession code is 1NEF.

Received 1 February; accepted 5 February 1996.

Acknowledgements
We thank W.A. Eaton and S. Bryant for stimulating discussions; R. Tschudin for technical support, F. Delaglio and D.S. Garrett for software support and C. Lowell for the cDNA clone of Hck. This work was supported by the AIDS Targeted Anti-Viral program of the Office of the Director of the National Institutes of Health (to A.B., G.M.C., A.M.G., S.J.S. and P.T.W.).

1. Shugars, D.C. *et al.* Analysis of human immunodeficiency virus type I nef Gene sequences present *in vivo*. *J. Virol.* **67**, 4639–4650 (1993).
2. Kestler, H.W. *et al.* Importance of the Nef gene for maintenance of high virus loads and for development of AIDS. *Cell* **65**, 651–662 (1991).
3. Kirchhoff, F., Greenhough, T.C., Brettler, D.B., Sullivan, J.L. & Desrosiers, R.C. Absence of intact nef sequences in a long-term survivor with nonprogressive HIV-1 infection. *N. Engl. J. Med.* **332**, 228–232 (1995).
4. Deacon, N.J *et al.* Genomic structure of an attenuated quasi species of HIV-1 from a blood transfusion donor and recipients. *Science* **270**, 988–991 (1995).
5. Daniel, M.D., Kirchhoff, F., Czajak, S.C., Seghal, P.K. & Desrosiers, R.C. Protective effects of live attenuated SIV vaccine with a deletion in the nef gene. *Science* **258**, 1938–1941(1992).
6. Cullen, B.R. The role of Nef in the replication cycle of the human and Simian immunodeficiency viruses. *Virology* **205**, 1–6 (1994).
7. Goldsmith, M.A., Warmerdam, M.T., Atchison, R.E., Miller, M.D. & Greene, W.C. Dissociation of the CD4 downregulation and viral infectivity enhancement functions of human immunodeficiency virus type 1 *Nef*. *J. Virol.* **69**, 4112–4121 (1995).
8. Salghetti, S., Mariani, R. & Skowronski, J. Human immunodeficiency virus type 1 Nef and p56lck protein-tyrosine kinase interact with a common element in CD4 cytoplasmic tail. *Proc. Natl. Acad. Sci. USA* **92**, 349–353 (1995).
9. Greenway, A., Azad, A. & McPhee, D. Human immunodeficiency virus type 1 Nef protein inhibits activation pathways in peripheral blood mononuclear cells and T-cell lines. *J. Virol.* **69**, 1842–1850 (1995).
10. Saksela, K., Cheng, G. & Baltimore, D. Proline-rich (PxxP) motifs in HIV-1 Nef bind to SH3 domains of a subset of Src kinases and are required for the enhanced growth of Nef+ viruses but not for down-regulation of CD4. *EMBO J.* **14**, 484–491 (1995).
11. Lee, C.-H. *et al.* A single amino acid in the SH3 domain of Hck determines its high affinity and specificity in binding to HIV-1 Nef protein. *EMBO J.* **14**, 5006–5015 (1995).
12. Schwartz, O., Marechal, V., Danos, O. & Heard, J.M. Human immunodeficiency virus type 1 Nef increases the efficiency of reverse transcription in the infected cell. *J. Virol.* **69**, 4053–4059 (1995).
13. Clore, G.M. & Gronenborn, A.M. Structures of larger proteins in solution: three- and four-dimensional heteronuclear NMR spectroscopy. *Science* **252**, 1390–1399 (1991).
14. Bax, A. & Grzesiek, S. Methodological advances in protein NMR. *Acc. Chem. Res.* **26**, 131-138 (1993).
15. Grzesiek, S., Wingfield, P.T., Stahl, S.J., Kaufman, J.D. & Bax, A. Four-dimensional 15N-separated NOESY of slowly tumbling perdeuterated 15N-enriched proteins. Application to HIV-1 nef. *J. Am. Chem. Soc.* **117**, 9594–9595 (1995).
16. Grzesiek, S. & Bax, A. The importance of not saturating H_2O in protein NMR. Application to sensitivity enhancement and NOE measurements. *J. Am. Chem. Soc.* **115**, 12593–12594 (1993).
17. Freund, J., Kellner, R., Houthaeve, T. & Kalbitzer, H.R. Stability and proteolytic domains of Nef protein from human immunodeficiency virus (HIV) type 1. *Eur. J. Biochem.* **221**, 811–819 (1994).
18. Nilges, M., Clore, G.M. & Gronenborn, A.M. Determination of three-dimensional structures of proteins from interproton distance data by hybrid distance geometry-dynamical simulated annealing calculations. *FEBS Lett.* **229**, 317–324 (1988).
19. Freund, J. *et al.* A possible regulation of negative factor (Nef) activity of human immunodeficiency virus type 1 by the viral protease. *Eur. J. Biochem.* **223**, 589–593 (1994).
20. Huang, Y., Zhang, L. & Ho, D.D. Characterization of nef sequences in long-term survivors of human immunodeficiency virus type 1 infection. *J. Virol.* **69**, 93–100 (1995).
21. Ramakrishnan, V., Finch, J.T., Graziano, V., Lee, P.L. & Sweet, R.M. Crystal structure of globular domain of histone H5 and its implications for nucleosome binding. *Nature* **362**, 219–223 (1993).
22. Lim, W.A., Richards, F.M. & Fox, R.O. Structural determinants of peptide-binding orientation and of sequence specificity in SH3 domains. *Nature* **372**, 375–379 (1994).
23. Feng, S., Chen, J.K., Yu, H., Simon, J.A. & Schreiber, S.L. Two binding orientations for peptides to the Src SH3 domain: Development of a general model for SH3-ligand interactions. *Science* **266**, 1241–1247 (1994).
24. Wu, X. *et al.* Structural basis for the specific interaction of lysine-containing proline-rich peptides with the N-terminal SH3 domain of c-Crk. *Structure* **3**, 215–226 (1995).
25. Studier, F.W., Rosenberg, A.H., Dunn, J.J. & Dubendorff, J.W. Use of T7 RNA polymerase to direct expression of cloned genes. *Methods Enzymol.* **185**, 60–89 (1990).
26. Scharf, S.J., Horn, G.T. & Erlich, H.A. Direct cloning and sequence analysis of enzymatically amplified genomic sequences. *Science* **233**, 1076–1078 (1986).
27. Holtzman, D.A., Cook, W.D. & Dunn, A.R. Isolation and sequence of a cDNA corresponding to a src-related gene expressed in murine hemopoietic cells. *Proc. Natl. Acad. Sci. USA* **84**, 8325–8329 (1987).
28. Bax, A. *et al.* Measurement of homo- and heteronuclear J couplings from quantitative J correlation. *Methods Enzymol.* **239**, 79–105 (1994).
29. Brünger, A.T. *XPLOR Version 3.1: A system for Crystallography and NMR*, Yale University, New Haven, CT, USA (1992).
30. Garrett, D.S. *et al.* The impact of direct refinement against three-bond HN-CaH coupling constants on protein structure determination by NMR. *J. Magn. Reson.* B**104**, 99–103 (1994).
31. Kuszewski, J., Qin, J., Gronenborn, A.M. & Clore, G.M. The impact of direct refinement against proton chemical shifts in protein structure determination by NMR. *J. Magn. Reson.* B**107**, 293–297 (1995).
32. Carson, M. Ribbon models of macromolecules. *J. Mol. Graphics* **5**, 103–106 (1987).
33. Nicholls, A, Sharp, K.A. & Honig, B. Protein folding and association: insights from the interfacial and thermodynamic properties of hydrocarbons. *Proteins* **11**, 281–296 (1991).
34. Brooks, B.R. *et al.* CHARMM: a program for macromolecular energy minimization and dynamics calculations. *J. Comput. Chem.* **4**, 187–217 (1983).